The detector subsystem for the SXS instrument on the Astro-H observatory

F. S. Porter[a], J. S. Adams[a], G. V. Brown[b], J. A. Chervenak[a], M. P. Chiao[a], R. Fujimoto[c], Y. Ishisaki[d], R. L. Kelley[a], C. A. Kilbourne[a], D. McCammon[e], K. Mitsuda[f], T. Ohashi[d], A. E. Szymkowiak[g], Y. Takei[f], M. Tashiro[h], N. Yamasaki[f]

[a]NASA/GSFC, Greenbelt, MD , [b]Lawrence Livermore National Laboratory, Livermore, CA, [c]Kanazawa University, Kanazawa, Japan, [d]Tokyo Metropolitan University, Tokyo, Japan, [e]University of Wisconsin, Madison, WI, [f]ISAS/JAXA, Sagamihara, Japan, [g]Yale University, New Haven, CT, [h]Saitama University, Saitama, Japan

ABSTRACT

The Soft X-ray Spectrometer (SXS) instrument on the Astro-H observatory is based on a 36 pixel x-ray calorimeter array cooled to 50 mK in a sophisticated spaceflight cryostat. The SXS is a true spatial-spectral instrument, where each spatially discrete pixel functions as a high-resolution spectrometer. Here we discuss the SXS detector subsystem that includes the detector array, the anticoincidence detector, the first stage amplifiers, the thermal and mechanical staging of the detector, and the cryogenic bias electronics. The design of the SXS detector subsystem has significant heritage from the Suzaku/XRS instrument but has some important modifications that increase performance margins and simplify the focal plane assembly. Notable improvements include x-ray absorbers with significantly lower heat capacity, improved load resistors, improved thermometry, and a decreased sensitivity to thermal radiation. These modifications have yielded an energy resolution of 3.5-4.0 eV FWHM at 6 keV for representative devices in the laboratory, giving considerable margin against the 7 eV instrument requirement. We expect similar performance in flight.

Keywords: X-ray, detector, spaceflight

1. INTRODUCTION

The Soft X-ray Spectrometer (SXS) instrument will be launched as part of the Astro-H Observatory[1] in early 2014. The SXS is a collaboration between NASA, JAXA, SRON, and the University of Geneva, and is described in detail in this proceedings[2]. Briefly, the SXS is a cryogenic non-dispersive x-ray spectrometer based on x-ray microcalorimeter detectors developed for the XRS instrument on the Astro-E2 (Suzaku) observatory. The detectors are operated at 50 mK to maximize their sensitivity and minimize the heat capacity to give extremely high signal to noise. The detectors for the Astro-E2 program are described in detail by Stahle et al.[3] Briefly, a microcalorimeter detector detects individual x-ray photons by absorbing them in an x-ray absorber and using a very sensitive thermometer to measure the heat produced by the thermalization of the primary photo-electron, and the ionized atom in the absorber. The thermometer is sensitive enough to measure the energy of the incident x-ray with a resolving power of about 1500 at 6 keV.

The SXS detectors are cooled to 50 mK using a multistage cooling system[4]. This consists of redundant mechanical Stirling cycle shield coolers that provide thermal shields down to 25K. A liquid helium tank at 1.3 K provides the final precooler stage for a two stage adiabatic demagnetization refrigerator (ADR) that provides the final cooling to 50mK. To provide redundancy for the liquid helium system, a 4.5 K Joule-Thomson (JT) cooler and an additional ADR stage can provide the 1.3K interface for the two-stage ADR should the liquid helium system fail. The redundant cooling system also allows the SXS to continue operating well beyond the required 3-year life of the cryogens, limited only by the life of the mechanical coolers.

In this document we will describe one of the central components of the SXS, the detector subsystem. An overview of the subsystem is shown in Figure 1. The detector subsystem consists of the microcalorimeter array, the anti-coincidence detector, the mechanical housing attached to 50 mK, the first stage amplifiers, the detector bias dividers, and the thermal isolation structure that allows the subsystem to be mechanically supported from 1.3K. The following sections describe each of these components in detail.
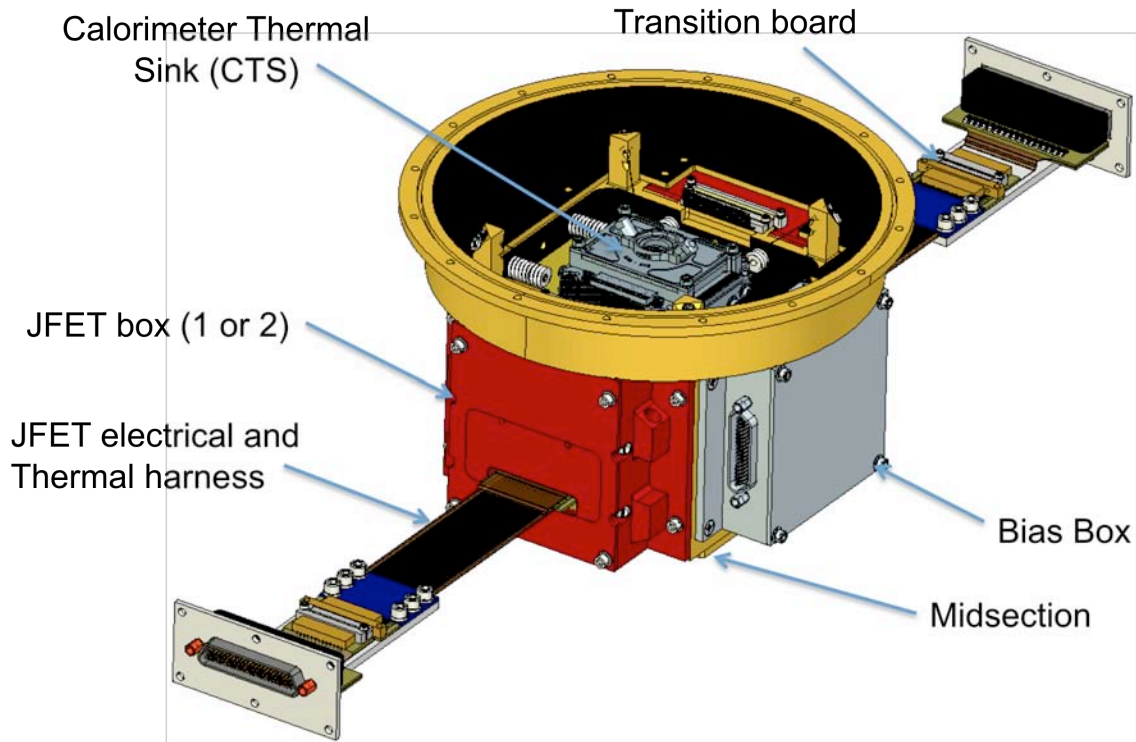
Figure 1. A Solid model of the SXS detector subsystem. For scale, the central module is about 6" in diameter. The detector array and the anti-coincidence detector are housed in the CTS (center of figure), which is anchored at 50 mK. The outer structure is anchored to the LHe tank at 1.3K. Note that the JFET electrical harnesses have been shortened for clarity.

2. SXS MICROCALORIMETER ARRAY

The SXS Microcalorimeter focal plane consists of a 6x6 array of detectors ("pixels") on a 12x14 mm silicon die. There are also two pixels to one side of the main array on the die that can be separately illuminated to provide gain-tracking of the main array. Finally there are two pixels that are not thermally isolated from the detector die, that are used for diagnostics. Thus the SXS detector array has a total of 40 devices. The details of the device structure are described in detail by Stahle et al.[3], but briefly, the array is micromachined from a Silicon-on-Insulator (SOI) wafer to define the pixels. The device layer contains a thermal isolation structure machined into the silicon using deep reactive ion etching. Further the device layer of each pixel is ion-implanted to form the thermometers for the device. Finally, a thick x-ray absorber is affixed to polymer standoffs on the pixel to absorb and thermalize x-rays. The x-ray absorbers for the SXS are formed by MBE grown HgTe. HgTe has been used successfully in our detectors for the last 20 years and is a compromise between low heat capacity and efficient thermalization.

The detector arrays for the SXS consist of 814 μm pixels on an 832 μm pitch. These are larger than the 640 μm pitch used for the XRS instrument on the Astro-E2 observatory, but were actually manufactured during the XRS program as an alternative design. The longer focal length of the SXS (5.6 m vs. 4.5 m), necessitates a larger array to maintain the FOV at 2.9 x 2.9 arcminutes. The x-ray absorbers for SXS consist of 8.5 μm thick HgTe grown by EPIR and diced using reactive ion etching. An SXS detector array without absorbers is shown in Figure 2(a), and a partially assembled detector array showing the x-ray absorbers and the underlying pixels is shown in Figure 2(b).

Although the detector arrays for the SXS were manufactured during the XRS program, we have made several substantial improvements. On the ground, the performance of the detectors was limited by an extra linear term in the heat capacity of the HgTe on top of the expected Debye heat capacity. EPIR, using improved manufacturing processes, has provided us with material that exhibits no excess heat capacity[5]. Thus, even though the SXS detectors are 70% larger area, the energy resolution at 6 keV is actually improved from ~ 6 eV on XRS to ~ 4 eV FWHM on SXS. The improvement is

due to the lower heat capacity of the HgTe and our ability to operate the SXS at 50 mK instead of the 60 mK on XRS. An example of an SXS prototype detector operating in our laboratory at 50 mK is shown in Figure 3.
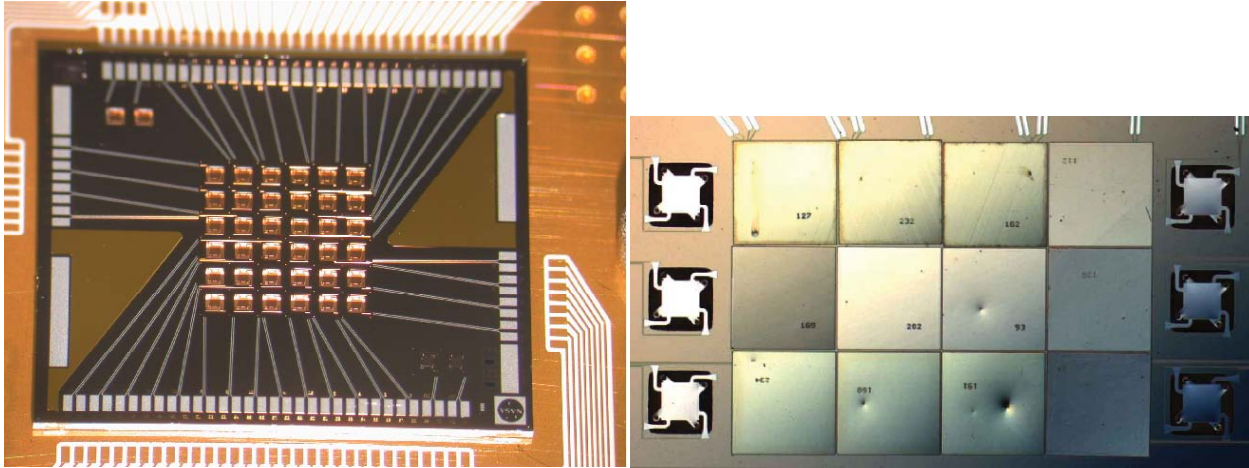

Figure 2. (a, left) SXS microcalorimeter detector array without the HgTe absorbers attached. Note the triangular gold heat sinks in the upper right and lower left. These are a substantial improvement to the XRS design that significantly reduce thermal crosstalk. (b, right) a partially assembled SXS detector array showing pixels with (center) and without (left and right) HgTe absorbers.

The performance of the XRS detectors in space[6] was slightly worse than on the ground (6.7 eV vs. 6.0 eV). The degradation is due to thermal crosstalk between cosmic rays interacting with the silicon frame of the detector die and the calorimeter pixels. For SXS we have added gold heatsinking layers to both the front and back of the detector die, and this has effectively eliminated the thermal cross talk in ground testing. We expect the performance of the SXS detector system to be the same in space as in our ground testing.
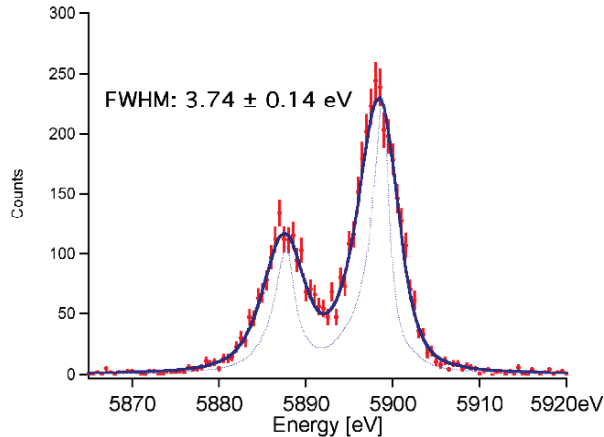

Figure 3. Spectrum of Mn Kα from an 55-Fe source measured with a prototype SXS detector system. This particular device yields an energy resolution of 3.74 eV FWHM at 6 keV. We have tested several dozen prototype devices and the performance ranges from 3.5-4.5 eV.

3. SXS ANTICOINCIDENCE DETECTOR

The SXS anti-coincidence detector (anti-co) is identical to that deployed in the XRS instrument on Astro-E2. The anti-co die for SXS is from the same fabrication lot as the XRS detector. This is described in detail in Kelley et al.[6]. For completeness we describe the SXS anti-co briefly here.

The SXS detector system uses a Low Voltage Silicon Ionization Detector (LVSID) anti-coincidence detector placed directly behind the detector array to veto events in the main-array due to minimum ionizing particles. A conceptual

drawing of this arrangement is shown in Figure 4. The same anti-co was used in the XRS instrument on Astro-E2. The XRS instrument operated for about 6 weeks on orbit before a flaw in the accommodation of the experiment caused the pre-mature loss of LHe and the end of the science capability of the instrument. The LVSID anti-coincidence detector, however, continues to operate after 5 years on orbit (launch July 10, 2005), with no sign of degradation in low-earth orbit (550 km) although the noise of the bias and readout has increased slightly since the solid Neon cryogen was exhausted after 22 months on orbit.
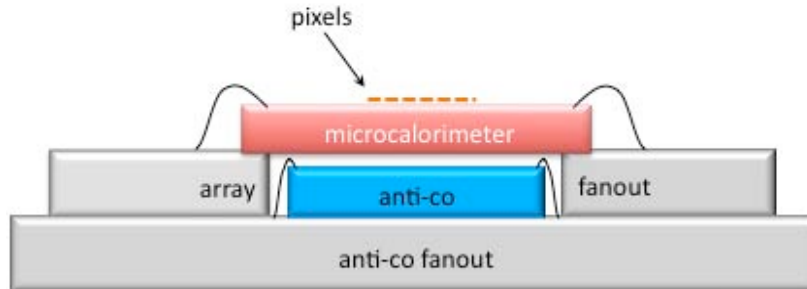

Figure 4. Schematic arrangement of the Astro-H/SXS microcalorimeter detector array and the LVSID anti-coincidence detector.

The SXS LVSID detector is a 1cm x 1cm x 0.5 mm square of high purity silicon with one side degenerately doped with boron and the other with phosphorous. The implanted regions are rounded at the corners and pulled back slightly from the edge of the device to eliminate uncontrolled field concentrations. A mechanical model using an actual SXS anti-co chip and its mounting board is shown in Figure 5. Although the design is essentially a PiN (p+-insulator-n+) diode, at low temperatures the carriers are completely frozen-out and the device operates purely as an ionization detector. The SXS anti-co is operated at low voltage, ~6V with no change in gain observed for biases above 2V, and is heat sunk along with the detector array at 50 mK. We use a simple read out scheme, very similar to the microcalorimeter detectors, which vastly simplifies the focal plane assembly. Higher performance could be achieved by using a charge amplifier and feedback to increase the speed of the detector, but this is unnecessary for the SXS instrument. A simplified schematic of the SXS readout is shown in Figure 6.
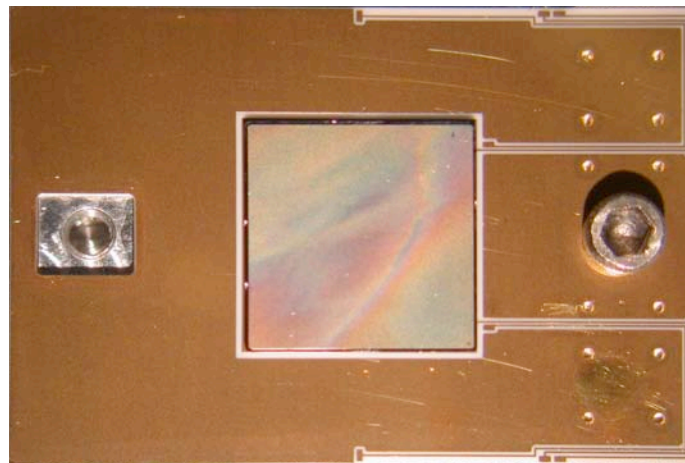

Figure 5. Mechanical model of the Astro-H/SXS LVSID anti-coincidence detector (center) attached to its gold plated high purity alumina mounting board. Note that the LVSID and mounting board are working flight parts assembled for bond shear testing. The LVSID die is 1.0 x 1.0 cm x 0.5 mm thick.

A pulse from an XRS LVSID anti-co detector due to a 60 keV gamma ray is shown in Figure 7. The only significant difference between the anti-co detectors on Astro-E2/XRS and Astro-H/SXS is in the pulse-processing algorithm and in the bias resistor. The bias resistors used for SXS speed up the fall time of the anti-co by about a factor of two compared to the pulse shown in figure 7 to about 130 μs fall time. On Astro-E2 the anti-co signal was compared to a defined threshold that was used to trigger a predefined veto window. On Astro-H the anti-co pulses are digitized and processed

using the same digital pulse processing algorithms as the main detector array. This allows the Astro-H/SXS anti-co to be used for spectroscopy and for more advanced veto windows than that on Astro-E2.
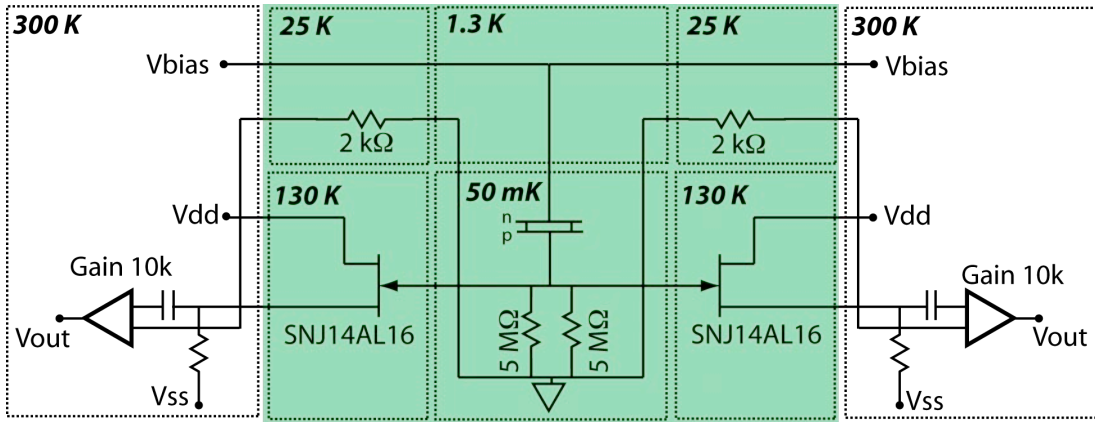

Figure 6. Readout circuit for the Astro-H/SXS LVSID anti-co detector. Since there is only a single anti-co detector, it is designed with redundant readout nodes. The thermal staging of each area is shown in bold and the areas shaded in green are contained within the detector assembly (DA).
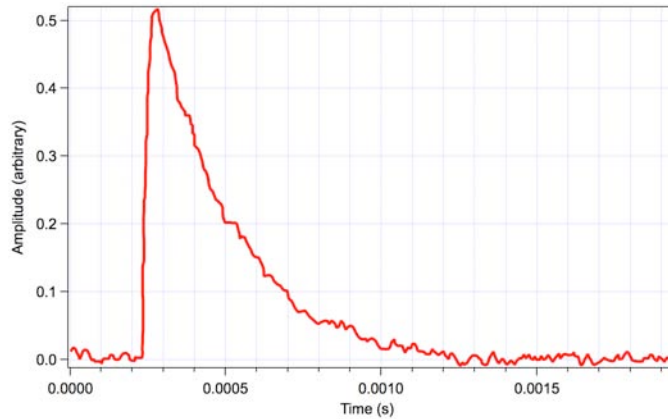

Figure 7. Single 60 keV gamma ray measured with the XRS LVSID anti-coincidence detector. The pulse has a risetime of 12 μs and a fall time of 260 μs, limited by the LVSID capacitance and the stray capacitance in the redundant readout circuit as shown in figure 2.

4. DETECTOR ASSEMBLY

The detector assembly (DA), shown in Figure 1, houses the detector array, and the anti-co detector and interfaces them, mechanically, electrically, and thermally to the rest of the SXS instrument. The unit is completely modular and requires only electrical cables, a 1.3 K mechanical support, and a flexible thermal strap to the 50mK ADR to operate the detector. A simplified electrical schematic of the detector readout is shown in Figure 8 with the areas contained in the detector assembly highlighted in green. Similarly, the simplified schematic for the anti-co detector is shown in Figure 6, with the detector assembly areas again highlighted in Green. The trick for building the detector assembly, and the part that required the most engineering, is to operate the 50 mK detector within a few centimeters of the 130K JFET trans-impedance amplifiers while keeping the heat loads on the 50 mK ADR, and the 1.3 K helium tank as low as possible. This is largely achieved by separately Kevlar suspending the 50mK detector stage and the JFETs inside modular subassemblies in the DA.

The local terminology for the subassemblies of the DA (referring to Figure 1) are Calorimeter Thermal Sink (CTS) for the 50mK detector housing, Midsection for the thermal and mechanical interface to 1.3 K, the JFET subassemblies which house the trans-impedance amplifiers, and the Bias box which contains the bias dividers. These are discussed briefly below. There are several complicating factors in the design. The first is that the impedance of the detectors under bias is about 30 MΩ so that they are exceedingly sensitive to capacitive fluctuations in the leads between the detector and the JFET. This translates into a microphonic contamination of the signal unless extreme care is taken in routing the leads. The solution is to tension the leads between the detector and the JFET so that their resonance frequency is well out of the detector band. The analog detector signals are rolled off with an 8-pole low pass filter at around 2 kHz and the resonance frequency of the leads is staged above that level.
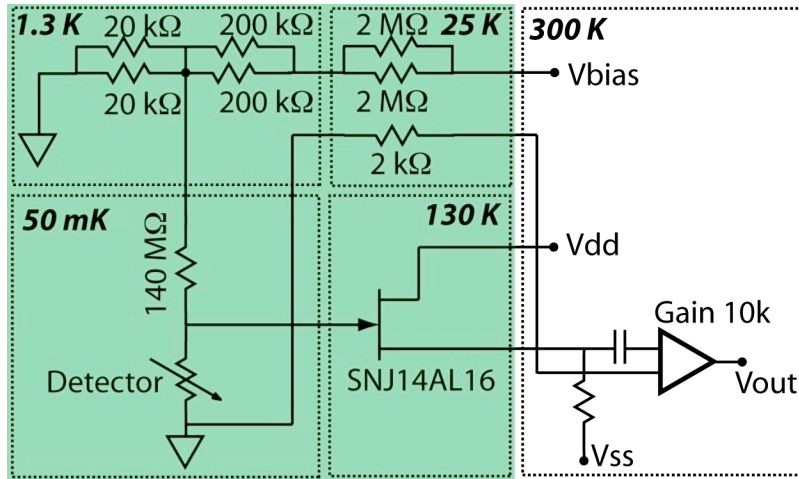

Figure 8. Simplified schematic of the SXS detector read-out circuit. The thermal staging of the components is shown in bold and the areas shaded in green are contained within the detector assembly (DA).
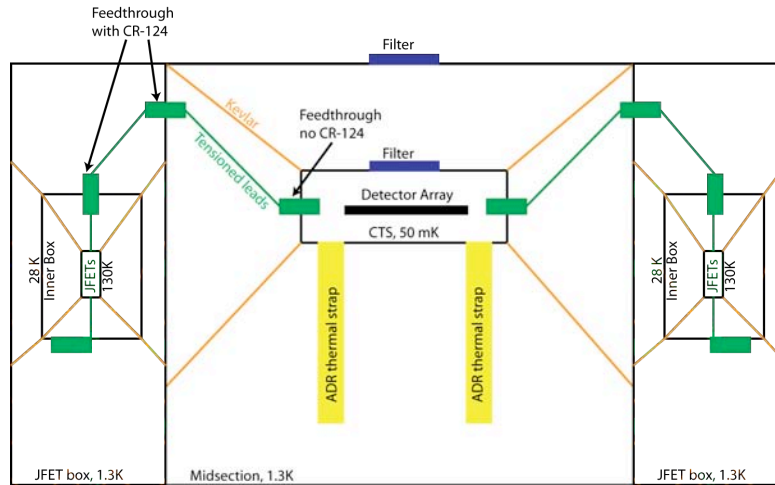

Figure 9. Schematic overview of the SXS Detector Assembly (DA) showing the tensioned Kevlar supports (orange) and the electrical leads and feedthrus (green).

A second complicating factor is that the detectors not only act as calorimeters but also as bolometers, i.e. they are sensitive to not just thermal transients but also to radiative power. To reduce the thermal radiation temperature in the 50mK CTS, several mitigations have been imposed. At the higher temperature stages, the connector leads are potted in Eccosorb CR-124 microwave attenuating epoxy. This damps the transmission of the thermal radiation energy from the 130K JFET inner cavity, and the 25 K JFET outer cavity into the midsection housing the CTS. The goal is to have the radiation temperature inside the midsection at 1.3K. Damping the 1.3K radiation into the CTS is not tractable as the heat capacity of the CR-124 is very high and would give the CTS a long thermal time constant. Thus the leads into the CTS are not damped. However, the inside lid of the CTS is coated with a ~1 mm thick coating of graphite loaded epoxy to

damp radiation inside the CTS. The gain stability of the XRS instrument was limited by the magnitude and stability of the radiation field inside the CTS, but the CTS cavity on the XRS was not damped at all and was presumably fairly high Q. We have employed damping inside the CTS in our ground experiment, the EBIT Calorimeter Spectrometer (ECS)[7] since 2007 and have seen nearly perfect gain stability. In fact we do not perform any gain drift correction for the ECS data.

The SXS DA has extensive heritage from the XRS DA[8]. The overall size and appearance of the two units is virtually identical. In addition, the design of the Kevlar suspension for both units is very similar. However, the SXS DA design has been modified to overcome deficiencies and lessons-learned from the XRS program. These include modifications that make the SXS DA much easier to assemble. Many of these changes are outlined here.
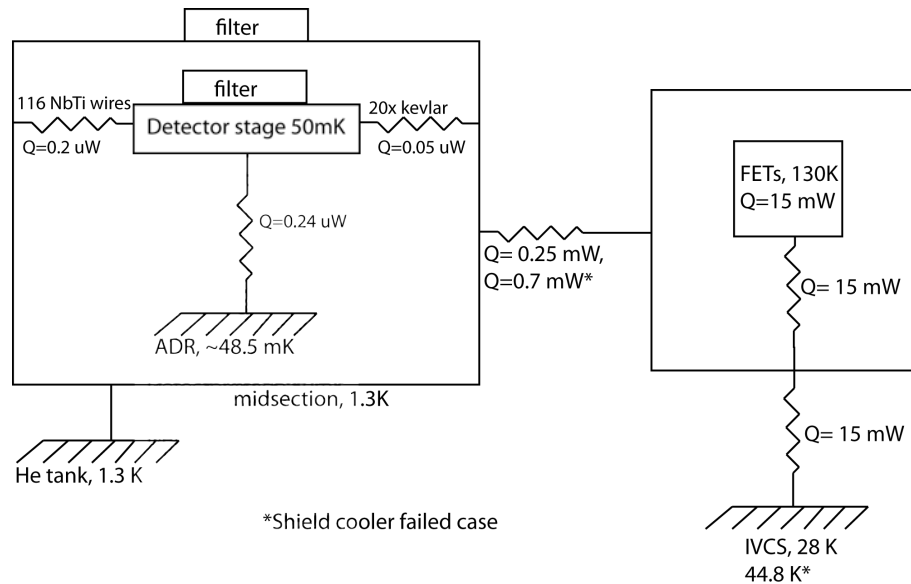

Figure 10. Thermal map of the detector assembly. The heat loads shown are calculating using our thermal model of the DA and have been verified by experiment using an XRS DA.

A schematic overview of the detector assembly is in Figure 9 showing, conceptually, the multiple Kevlar suspensions supporting the JFETs and the CTS. A thermal map of the DA is shown in Figure 10. Thermally, the challenge is to shunt the ~15 mW needed to heat and operate the JFETs at 130K away from the He tank and the CTS. This is described in section 4.2, but the requirement is a maximum of 380 µW on the helium tank and 0.5 µW on the ADR from all sources including both the bias supplies and the JFETs. That is a factor of 50 reduction of the JFET power to the He tank and a factor of 3000 to the detector stage.

The detector assembly is completely modular in that all of the subassemblies (midsection, bias box, JFET boxes) can be assembled, and removed easily without disturbing the detectors. The detectors can also be integrated and de-integrated from the CTS without major disassembly. In particular, the detectors are installed in the CTS after it is suspended and wired to the midsection. To install a detector, the lid of the CTS is removed, the detector and anti-co are then installed and wirebonded to the CTS. In addition, the DA is electrically segmented to minimize the loss of science due to a failure in any one component. The detectors themselves are completely electrically independent but the bias is organized into quadrants of 9 pixels each. Further, each of two JFET boxes has two independent JFET packages each with a common drain. Thus each quadrant of 9 pixels is electrically independent so that the loss of a bias circuit or a JFET drain does not affect the remainder of the channels. A simplified schematic of a quadrant is shown in Figure 11. Further the JFET boxes form a second segmentation into halves where the loss of a Kevlar suspension in a JFET box compromises only half the array. The segmentation into halves carries through to the analog and digital room temperature electronics, which are also completely independent all the way through the low voltage power supplies. The loss of any electrical component can at most compromise half the instrument.

Finally, we note that the scale of the detector assembly has changed between the XRS and SXS implementations. On XRS, only 32 of the possible 40 detectors channels (36 pixels, 2 calibration pixels, and 2 frame monitors) could be

readout as there were only 32 electrical channels. For SXS we increased the number of readout channels from 32 to 36 by adding an additional 4 JFETs into the JFET packages.
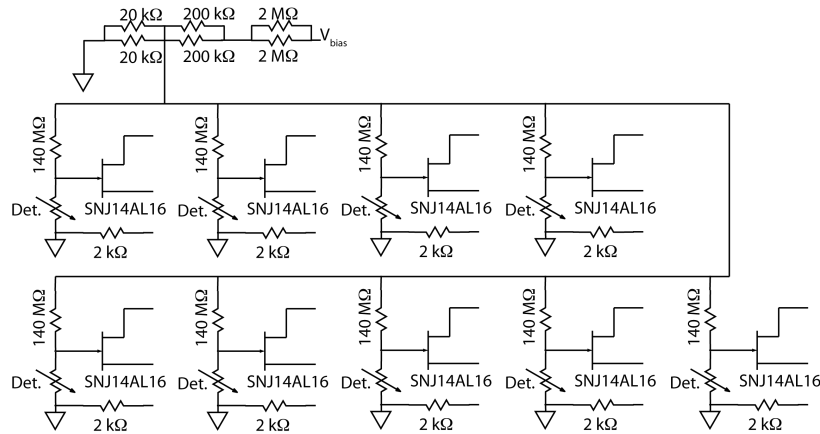

Figure 11. A simplified schematic of a detector "quadrant". The four quadrants of the DA are almost completely independent. Two quadrants are implemented in each of two JFET boxes. The JFET boxes are complexly independent from the detector array through the room temperature electronics. The loss of one JFET box and its associated two quadrants can, at most, compromise half the instrument.

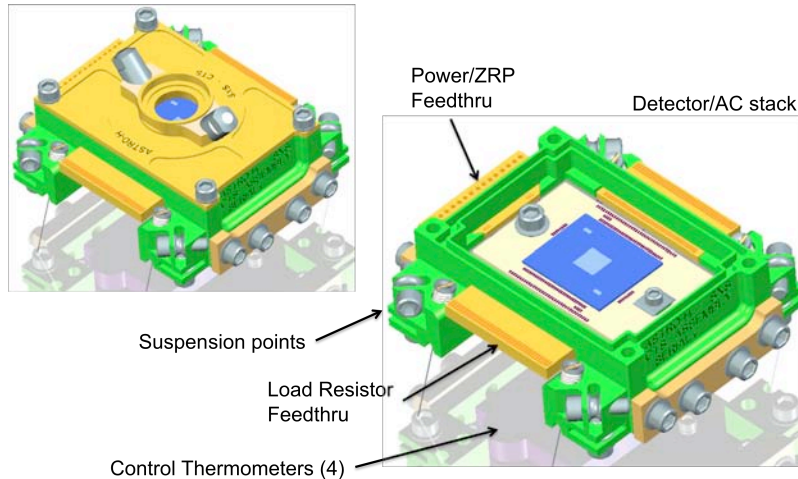## 4.1 Calorimeter Thermal Sink (CTS) and Midsection

Figure 12. The Calorimeter Thermal Sink (CTS) houses the detector array, the anti-coincidence detector, the load resistors, and the control thermometers at 50 mK. The CTS is shown with and without its cover. The CTS cover contains the first infrared blocking filter and a gain tracking 55-Fe x-ray source that illuminates one pixel to the side of the main array.

The CTS is shown in Figure 12. It contains the detector array, the anti-co detector, the 140 MΩ load resistors, and the ADR control thermometers that stabilize the CTS at 50mK during operation. The CTS is Kevlar suspended from the midsection and is electrically connected to the midsection with tensioned CuNi clad NbTi leads, 17 μm in diameter. The CTS is attached to the ADR using heavily annealed gold foils. The flexible link to the ADR is designed to minimize mechanical coupling between the two. The CTS is suspended with a first resonance frequency above 300 Hz, and the ADR with a first resonance frequency above 100 Hz, however there is virtually no coupling. The CTS has undergone substantial changes from the XRS design. The changes are centered around two themes, one is to reduce the susceptibility of the detectors to the magnitude and stability of the thermal radiation field inside the CTS cavity. The other is to simplify the complex wiring between the midsection, detector array, anti-co, bias supplies, and load resistors.

The CTS contains the microcalorimeter detector array mounted on a high purity (99%) alumina carrier board, and the anti-co detector that is also mounted on a high purity alumina carrier board. The boards are mounted in the interior

cavity of the CTS. One side of the board stackup is bolted to the CTS while the other is bolted to a BeCu flexure installed in the CTS. The flexure is designed to reduce the compressive stress on the detector boards due to the CTE mismatch between the copper CTS and the alumina detector boards. The flexure is designed to reduce the compressive load on the alumina board by an order of magnitude over two screws into the CTS at the same location. This is sufficient to keep the alumina boards and detector arrays well below their yield strength.

The SXS CTS wiring is planar, e.g. the electrical signals radiate outward from the detector boards, through the feedthrus to the tensioned leads to the midsection. The XRS CTS had the load resistors on the underside of the CTS structure requiring intricate three dimensional wiring to bring the bias from the bias box, to the load resistors and then back to the detectors on the inside of the CTS cavity. The SXS CTS brings that wiring into one plane by placing the load resistors inside the two feedthrus that bring the detector signals to the tensioned JFET wiring. The CTS feedthrus are 96% alumina with a cavity to house the load resistors. The feedthrus are gold coated with buried wiring to minimize the open area for radiative transmission through the feedthru. In this scheme, a 3rd feedthru is required that passes the detector and anti-co bias from the bias box tensioned leads to the anti-co detector and the microcalorimeter load resistors. The biases are passed between the bias feedthru (Power/ZRP in Figure 12) and the two load resistor feedthrus using traces on the anti-co carrier board. The final assembly process is significantly easier than for the XRS instrument due to the elimination of the complex three-dimensional wiring scheme. The SXS CTS and midsection wiring is a single plane of tensioned leads and board to board wirebonds.
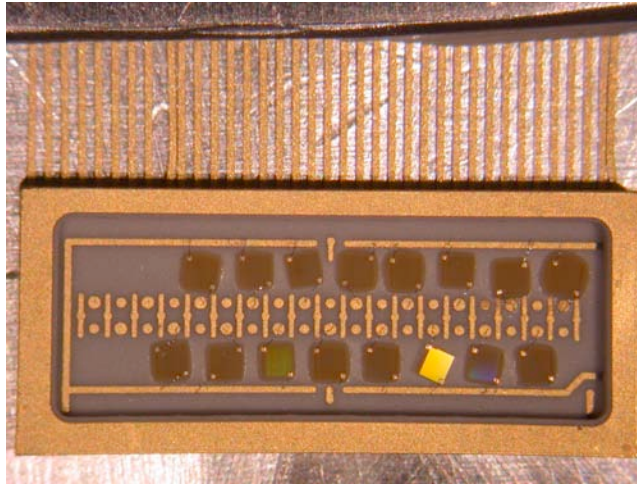

Figure 13. The SXS load resistors are contained within two of the three CTS electrical feedthrus. A partially populated bond-shear test model is shown using a flight load resistor board and flight Sichrome load resistors.

A key element in reducing the complexity of the CTS wiring layer is a change from Nichrome load resistors to Sichrome. The Nichrome load resistors from Minisystems, inc. that were used on XRS, had a maximum value of 30 MΩ per 1.5x1.5 mm die. Three dice were used per detector channel requiring a total of 96 dice for the XRS CTS assembly. The only available real estate for these devices was on the underside of the CTS. For SXS, we switched to Sichrome resistors, again from Minisystems. Sichrome resistors are available with much higher sheet resistivity although there is a slight temperature coefficient. For SXS we are using 100 MΩ resistors, Sichrome on quartz, in 1mm x 1mm die. Thus only one die per channel is required and the resistors are small enough to enclose inside the CTS feedthrus. One of the CTS feedthrus with load resistors installed is shown in Figure 13. The Sichrome load resistors are 100 MΩ at room temperature and about 140 MΩ at 50 mK. We conducted extensive testing of these devices in the laboratory and observed no non-ohmic behavior, i.e. the noise is pure Johnson noise at least from 5 Hz to 2 kHz. However, the temperature coefficient increases drastically at low temperature to between 50 and 70 MΩ/K at 50 mK. This affects the bias stability of the detectors. However if the load resistors are controlled to better than 100 μK RMS then the affect on detector noise is negligible. The requirement on CTS temperature stability is 2.5 μK RMS so this condition is easily met and does not drive the CTS temperature stability requirement. We also tested several SXS detectors with both Nichrome and Sichrome load resistors in our test ADR and found no difference in detector performance between the two. The Sichrome load resistors are now standard in our test systems and will be used for the SXS DA.

The thermal radiation environment within the midsection cavity and the CTS cavity had several undesirable effects during the XRS program. First, the control thermometers were mounted on the outside of the CTS and were formed with RuO2 thermistors enclosed in a gold plated copper bobbin with PhBr leads wound around the bobbin and staked with Armstrong A12 epoxy. As we have seen in other laboratory systems, the epoxy encapsulation of the leads has a very high emissivity and basically absorbs enough ambient radiation to heat the leads. The leads can then add a thermal load to the thermometer that competes with the heat sinking of the thermometer to the housing. In other systems we have seen thermometers that run as much as 50 mK warmer than the bobbin at 50 mK. On XRS, the thermometers ran within a few mK of the housing temperature but the two control thermometers and the two monitor thermometers were affected by the midsection cavity radiation and drifts in the temperature of that radiation field affected the control point of the ADR and thus the detector temperature. This effectively produced a gain drift of the detector vs. time as the midsection cavity radiation was not stable. The addition of a small copper shield over the potted thermometer bobbin, completely eliminates this affect in our laboratory cryostats. For SXS the two control and two monitor thermometers are located in a completely enclosed thermometer housing underneath the CTS which should have a radiation temperature close to 50 mK. This is designed to completely eliminate the problem as it has on our ECS instrument.

In addition, the XRS detectors themselves displayed a bolometric sensitivity to the radiation temperature in the CTS cavity and different detectors appeared to have different sensitivity depending on how well they shielded each other, effectively forming planar microwave antennas. On XRS, we observed a strong relationship between detector gain and He tank temperature, and a somewhat smaller affect from other parts of the cryostat. For SXS we have taken two approaches to solving this problem. The first is to apply a thick layer of graphite-loaded epoxy to the inside of the CTS cover in an effort to reduce the Q of the CTS cavity. We have successfully used this method on our ECS ground experiment that now shows no appreciable gain drift. In addition we control the temperature of the DA midsection using the heat flow from the ADR system to within 1 mK RMS over 10 minutes. This requirement maintains the detector performance within the system requirements even if we have made no improvement in the detector or thermometer sensitivity.

4.2 Junction Field Transistor (JFET) boxes

The JFET boxes for Astro-H/SXS are very similar to the JFET boxes used for XRS. The overall size and construction is the same with minor improvements to the Kevlar suspension and the organization of the wiring. The biggest change is the incorporation of two additional JFET channels in each box to bring the total DA channel count from 32 to 36. A picture of an Astro-E2 JFET box is shown in Figure 14.
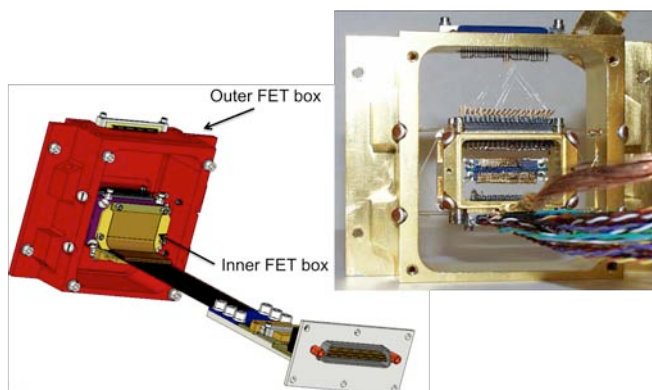

Figure 14. An SXS JFET module (left) and an almost identical XRS JFET module (right). The 130K JFETs themselves are in the center of the picture (right) and are Kevlar suspended from a 25K structure (center) which in turn is suspended from an outer 1.3K structure.

A JFET box is composed of two ceramic JFET packages each housing 10 JFETs. A JFET package, which also includes a heater and thermometer for temperature control, is shown in Figure 15. The two JFET packages are mounted to an aluminum plate that is Kevlar suspended inside a small gold plated aluminum box with two electrical feedthrus potted with Eccosorb CR-124. The aluminum "inner" box is thermally anchored to the Inner Vapor Cooled Shield (IVCS) of the SXS cryostat at ~25K. This allows us to shunt most of the 15 mW of heat generated at the JFET packages to a higher

temperature stage in the cryostat and not to the He tank. The total heat load on the He tank, from all sources, is below 1 mW. The inner JFET box is in turn Kevlar suspended to an "outer" JFET box that is anchored to the 1.3K DA midsection. This arrangement is shown schematically in Figure 9 and in the picture in Figure 14. The JFETs are wired to the inner box and then to the outer box using tensioned 20 μm diameter CuNi coated 304 stainless steel wire which provides good solderability, high strength, and low thermal conductivity.
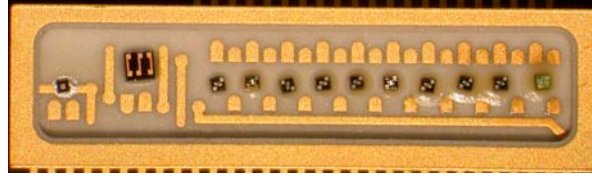

Figure 15. An SXS JFET package consisting of (left to right) a thermometer, a heater, and 10 JFETs. The detector assembly contains four such packages with a total of 36 detector channels, 2 anti-co channels, and 2 unwired spares. The package is about 2cm wide.

We carefully measured the heat load from the JFET box to the helium tank by mounting an XRS JFET box on a He-3 refrigerator where we had previously carefully measured the load curves. The results are shown in Figure 16 and were used to verify our thermal model. The thermal performance of the SXS FET box will be identical.

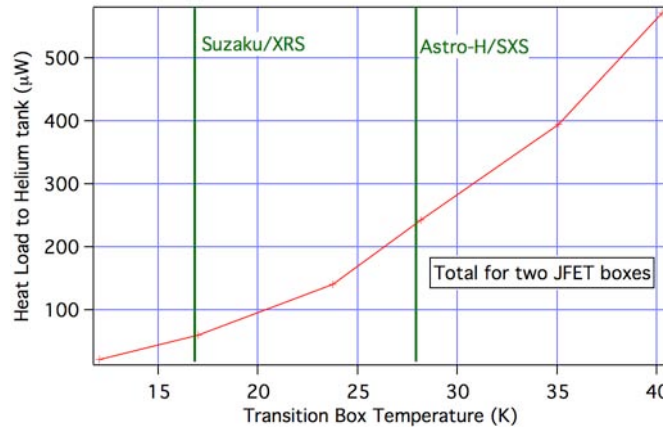Figure 16. The heat load from two SXS JFET boxes to the He tank as a function of the inner box heat sink (termed transition box in the figure) temperature. Most of the 15mW generated at the JFET modules is shunted to this heat sink. However, the higher the heat sink temperature, the higher the load on the He tank.
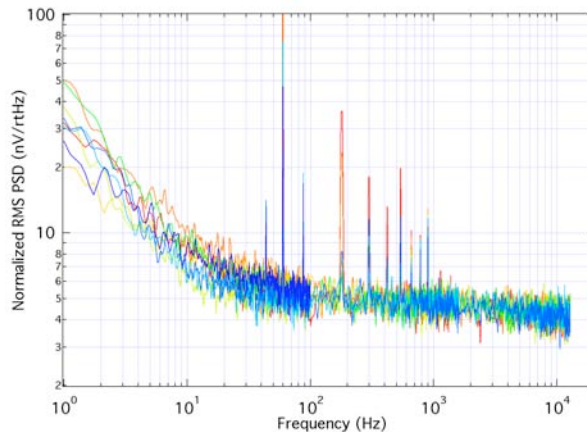

Figure 17. Measured noise performance of an SXS engineering model JFET module at 130K.

The JFETs used in the SXS are InterFET SNJ14AL16. The JFETs are about 4-5 nV/rtHz above 10 Hz in our measurements at 130 K as shown in Figure 17. We have successfully used these JFETs on both the XRS and SXS programs beginning in 1992 when the JFETs were manufactured (we have also procured a 2nd batch manufactured in 2009). The JFETs operated successfully for two years on orbit during the XRS program, long after the liquid helium was exhausted. No degradation of the JFETs was observed on-orbit. The JFETs are operated at 130K since this is approximately the minimum noise operating temperature for these devices. When the JFETs are operated slightly colder they start to exhibit generation-recombination noise as the carriers have begun to freeze-out.

The JFET source followers in the SXS reduce the impedance of the detectors from 30 MΩ to the 2 kΩ output impedance of the JFET. Thus the microphonic sensitivity of the DA effectively ends at the JFET and the harnessing beyond the DA does not need to be controlled for microphonics.

5. NOISE BUDGET

The detector performance requirement for the SXS is 7.0 eV FWHM at 6 keV with a goal of 4 eV. In fact the SXS detectors have only a minimal dependence of energy resolution on energy. They are slightly better at low energies and slightly worse at high energies, with the net effect being about 20% from 1 to 10 keV. The energy resolution of the SXS detectors is dominated by phonon noise, or the noise associated with thermal transport in the weak thermal link between each pixel and the silicon heat sink. However, many system parameters affect the overall performance of the detectors, not just the intrinsic resolution of the detectors themselves. We sum the uncorrelated contribution of all the system contributions to arrive at the expected system performance. We also hold margin for each system contribution and the system as a whole to assure that the overall performance requirements are met. The resulting apportionment of system noise between the various SXS subsystems is summarized in the SXS noise budget, which is given in Table 1 for the Microcalorimeter detector array and in Table 2 for the Anti-coincidence detector. The apportionment in the noise budget between the SXS subsystems is complex and won't be detailed here, and the budget and margins continues to evolve as the actual performance of each subsystem is measured. However, we have significant margin against the 7 eV full SXS requirement with our best estimate based on noise allocations of 4.6 eV and we routinely measure 4 eV or better in our laboratory systems that also include most of the same system noise sources.

Table 1. SXS Microcalorimeter detector noise budget. The Xbox is the room temperature analog electronics, the PSP is the room temperature digital electronics that calculates the energy of each event, and the ADRC is the ADR temperature controller.

noise budget (nominal bias)		allocation (eV)	in units measured	expected	basis	expected (in eV)
		eV FWHM				
base	ideal model	2.7				
detector system budget						
	excess broadening	3.5	3.5 eV	<2.5 eV	lab	2.5
	sub-mm photon noise	2	140 fW from 1.8K	<50 fW	XRS model	1.2
	JFET noise	2	9 nV/rt(Hz) white	4 nV/rt(Hz) white	XRS	0.8
			16 nV/rt(Hz) 1/f at 10	4 nV/rt(Hz) 1/f at 10		
	cosmic-ray heating	3	XRS sensitivity	10% XRS sensitivity	better heat sinking	0.3
	microphonics	1.2	12 Hz high S/N BW loss	0 Hz hi S/N BW loss	XRS	0.0
other subsystems						
ADRC	temperature control	1.2	2.5 uK RMS	1.0 uK RMS	heritage	0.5
Xbox	bias noise (at R_Load)	0.2	7.3 nV/rt(Hz)	0.5 nV/rt(Hz)	BB+Johnson	0.0
Xbox	bias stability	1.8	0.015% RMS	0.007% RMS	BB	0.8
Xbox	amplifier noise	1	5 nV/rt(Hz)	2 nV/rt(Hz)	BB	0.4
			5 nV/rt(Hz) 1/f at 10	2 nV/rt(Hz) 1/f at 10		
XBox	gain stability	2	0.012% RMS	0.01% RMS	BB	1.7
PSP	computational error	0.5	0.5 eV	0.0 eV	XRS	0.0
ADRC	~1K interface stability	1	1 mK RMS	1 mK RMS	model	1.0
RESERVED MARGIN		0.7				0.0
	RSS of base and noise	7.0				4.6

Table 2. SXS Anti-coincidence detector noise budget.

anti-co noise budget	keV FWHM				
	allocation	in units measured	expected	basis	expected (in keV)
	(keV)				
detector system budget					
JFET noise	2.5	9 nV/rt(Hz) white #	4 nV/rt(Hz) white +	XRS	1.1
		16 nV/rt(Hz) 1/f at 10 #	4 nV/rt(Hz) 1/f at 10		
other subsystems					
Xbox bias noise	14.1	75 nV/rt(Hz) *	40 nV/rt(Hz)	BB	7.5
Xbox amplifier noise	1.3	5 nV/rt(Hz) #	2 nV/rt(Hz) white +	BB	0.5
		5 nV/rt(Hz) 1/f at 10 #	2 nV/rt(Hz) 1/f at 10		
RESERVED MARGIN	8				0.0
RSS of base and noise	16.5				7.6

6. SUMMARY

The Detector Subsystem for the SXS instrument is an evolutionary descendent of the Detector Subsystem for the XRS instrument on the Suzaku observatory, but with a number of critical improvements both to overcome shortcomings in the XRS design, and to simplify the assembly of this complex instrument. The improvements to the detector subsystem and the SXS cryostat and electronics, incorporate all the lessons we learned in the XRS program including the redundancy of the instrument cooling system from room temperature to 1.3K. The resulting SXS instrument is robust, modular, and has no defined lifetime. The design of the cryostat and the liquid helium load is for a minimum three year lifetime, however the mechanical coolers allow the instrument to continue to operate after the liquid helium is exhausted. We are currently manufacturing an engineering model detector subsystem that will be integrated into a full engineering model SXS instrument in the spring of 2011. The final SXS instrument will be assembled in 2012 for launch in early 2014. The end result will be a high performance spatially resolved x-ray spectrometer that will be the workhorse for x-ray astrophysics until the proposed launch of the International X-ray Observatory sometime in the next decade.

REFERENCES

[1] Takahashi, T., Mitsuda, K., and Kelley, R. L., "The Astro-H Mission", Proc. SPIE 7732 (this proceedings) (2010).
[2] Mitsuda, K., et al., "The high-resolution x-ray microcalorimeter spectrometer system for the SXS on ASTRO-H", Proc. SPIE 7732 (this proceedings) (2010).
[3] Stahle, C. K., et al., " Next generation of silicon-based x-ray microcalorimeters", Proc. SPIE, 4851, 1394 (2003)
[4] Fujimoto, R., et al., "Cooling system for the soft x-ray spectrometer (SXS) onboard ASTRO-H", Proc. SPIE 7732 (this proceedings) (2010).
[5] R. L. Kelley et al., "Ion-Implanted Silicon X-Ray Calorimeters: Present and Future", JLTP, 151, 375-380 (2008).
[6] R. L. Kelley et al., "The Suzaku High Resolution X-Ray Spectrometer (XRS)", PASJ, 59, S77-S112 (2007).
[7] Porter, F. S. et al., "Performance of the EBIT Calorimeter Spectrometer", Rev. Sci. Inst., 79 (2008) 10E307-10E307-4.
[8] Porter, F. S., et al., "The detector assembly and the ultra low temperature refrigerator for XRS", Proc. SPIE 3765 (1999) 729.